Semi-analytical approch for brake squeal of a rail pad

Jaehyeon Nam and Jaeyoung Kang

School of Mechanical Engineering, Inha University, Incheon 22212, Korea

Abstract   In this study, a semi-analytical pad model was developed to analyze the causes and mechanism of brake squeal of a rail pad in a railway brake system. A complex eigenvalue analysis was performed by developing the equation of motion of the contact area using a semi-analytical model. As a result, dynamic instability was indicated by the mode-merging of the z-translation mode and flexible mode of the rail pad. In addition, the z-translation mode of the rail pad has a large frequency change when increasing the contact stiffness, and mode-veering is generated by the surrounding flexible mode along the frequency loci. Therefore, z-translation mode is predicted to be major mode that generates the mode-coupling instability.

1. Introduction

Friction noise is one of the most frequent problems in mechanical systems and has been studied for a long time in the vibration field [1-6]. In the past, studies predicting friction noise were performed mainly using spring mass friction models. Recently, however, finite element analysis (FEA) has been used to predict friction noise problems in friction systems based on actual geometries.

The squeal generated in an automotive brake system is a representative example of a friction-induced vibration problem. Frictional forces are defined between a rotating disc and pad, and the dynamic instability of the system is predicted by complex eigenvalue analysis [7-12]. Nam et al. [13, 14] predicted friction noise using FEA in a model of a lead screw and ball joint and verified the results through tests. However, when using commercial software, repetitive tasks and much time are required to demonstrate the mechanism of the friction noise. On the other hand, a purely theoretical model can be used to obtain exact solutions but is limited to systems without complex geometry.

To overcome this problem, semi-analytical models have been proposed to perform various parametric studies on complex geometries by applying an FE model to a theoretical model. This method can analyze complex system geometries using the FE model, and a friction-contact model is used as a mathematical model. Kang [15-17] investigated the major factors in squeal using a semi-analytical model in various systems, including an automotive disc brake system. A comprehensive disc brake vibration model was also developed using a theoretical model, and a nonlinear analysis of brake squeal was conducted. Studies on railway brake squeal have focused on the rotor mode of disc brake systems and wheel brake systems [9, 18-22]. However, there have been relatively few studies on squeal noise due to the rail pad.

The rail pad is designed as independent or separable rather than solid type to cool the heat generated by friction and minimize frictional properties due to debris. The geometric shapes mentioned above can generate a variety of vibration modes compared to automotive brake pads [3, 9, 19, 22]. Kang [23, 24] studied the mode-coupling instability in rigid modes for automotive pads with a semi-analytical model using theoretical and FE models. However, there have been no studies on the squeal propensity for the rigid mode of a rail pad.

The squeal noise generated on a railway can generate a wide range of friction noise as a result of various mechanisms [25]. In particular, mode-coupling instability is a major mechanism of frictional noise that is usually generated at closely spaced frequencies, such that dynamic
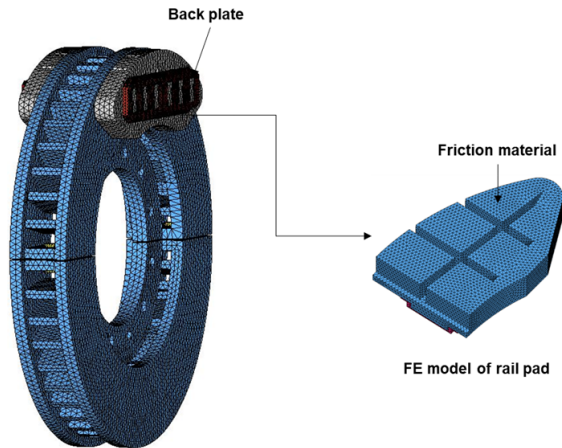
Fig. 1. Railway brake assembly and FE model of a rail pad.

instability mainly occurs in pair modes [4, 9, 13, 14, 23, 26, 27]. Nam et al. [13] studied the dynamic instability of lead screw systems. The dynamic instability due to mode-coupling and negative slope is caused by bending pair mode and torsion mode, respectively. In addition, propensity for each squeal mechanism was experimentally verified. Huang et al. [27] investigated the squeal of automotive drum brake. They performed a sensitivity analysis to describe the difference between the mode undergoing veering and crossing for conditions expressing mode-coupling instability. In addition, the mode softening mechanism was verified through eigenvector sensitivity. This study predicts the squeal noise generated in the pad of a railway brake system based on friction-contact theory, which has been used in a semi-analytical model. We describe the mode-coupling instability generated in a single rail pad using a model of an actual rail pad.

The semi-analytical friction noise model was developed while focusing on the mode-coupling instability due to the rigid mode of the rail pad. We also investigated the cause of the dynamic instability due to the rigid mode in the rail pad and the squeal mode through a sensitivity analysis and the modal contribution factor (MCF). We analyzed the squeal propensity using a stability analysis in terms of mode-coupling instability and predicted the squeal noise generated in the pad of a railway brake system.

## 2. Modeling of railway brake pad

2.1 Material properties

To analyze the dynamic instability generated in a rail pad, an FE model was constructed for a commercial railway brake system and rail pad, as shown in Fig. 1. The pad of the railway brake system is larger than an automotive brake pad, and the contact area is complicated. The model is based on an actual pad, which is divided into left and right sides.

To increase the reliability of the FEA, a hammering test was performed on the rail pad, as shown in Fig. 2. The FEA model was constructed based on the results of the modal analysis.
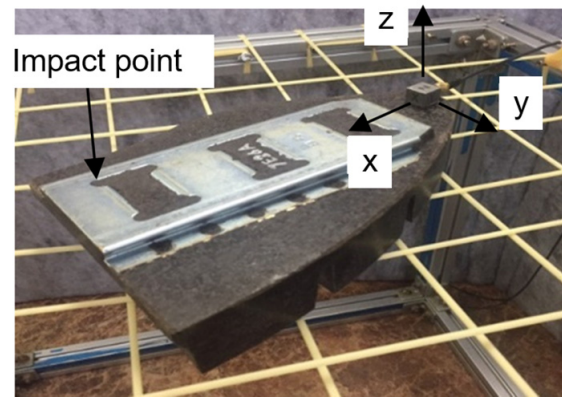
(a)
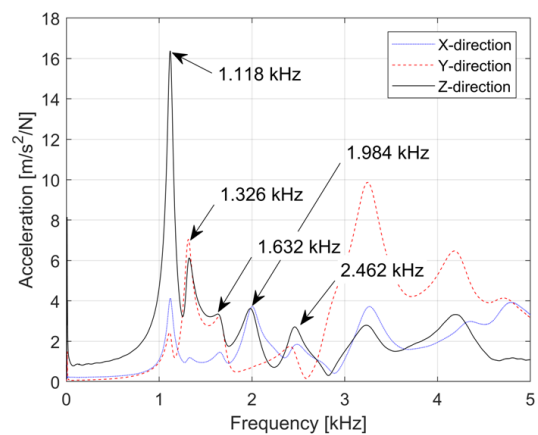
(b)

Fig. 2. Hammering test of a rail pad: (a) test setup; (b) results.

The frequency response using the hammering test was tested on a flexible jig to measure the free-free boundary conditions of the rail pad. An impact force was applied in the -z direction, and the frequency response was measured using a three-axis accelerometer. The setup of the hammering test is shown in Fig. 2(a), and the test results are shown in Fig. 2(b).

The results of the hammering test show about seven peaks at up to 4.5 kHz and were compared with the results of a modal analysis. The results of comparison between modal testing and modal analysis are shown in Table 1 and are indicated mode shapes for the five lowest frequency modes of free boundary condition. The mode shapes are dominated by the translation mode of cube component and bending mode of rail pad. In general, the back plate of the rail pad and the friction material are made of steel and organisms, respectively. Table 2 shows the material properties of the rail pad obtained as a result of the impact hammer test. The material properties had about 10 % average error based on the z displacement.

The contact stiffness was calculated from Young's modulus of the friction material, which was measured during the hammering test. The uniform contact stiffness was modeled as the numerical integration of contact area. The contact stiffness for the contact area estimated by the impact experiment was calculated to be 1.48e11 N/m^3 (100 %). A parameter study for

Table 1. Results of modal test.

Mode	Mode shape	FEM [kHz]	Test [kHz]	Error [%]
1		1.189	1.118	6
2		1.364	1.326	2
3		1.818	1.632	11
4		2.158	1.984	8
5		2.335	2.462	5

Table 2. Material properties of rail pad.

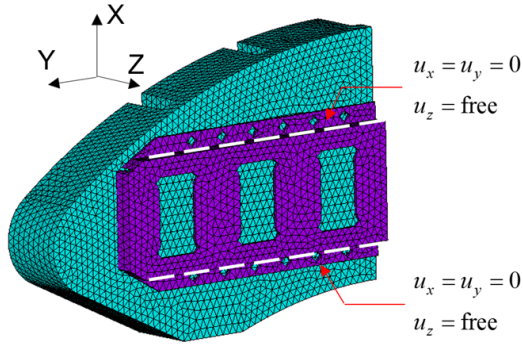| Components	Density [kg/m^3]	Young's modulus [Gpa]	Poisson's ratio
Back plate	7850	200	0.3
Friction material	2516	5.2	0.25

Fig. 3. Boundary condition of rail pad.

mode-coupling instability was also performed.

2.2 Derivation of equation of motion

The boundary conditions of the rail pad are shown in Fig. 3. The x displacement and the y displacement above and below the back plate are fixed, and the z displacement is free. These boundary conditions are similar to those of the actual rail pad, and the z-translation mode is generated due to free boundary conditions in the z direction. A linear stability analysis was also performed using a mode shape that satisfies the boundary conditions with FEM due to the complicated geometry.

The disc is assumed to be rigid and to rotate at a constant rotation speed (Ω). The sliding velocity of the disk on the contact point in the pad is defined as $\mathbf{v_d}$. As shown in Fig. 4, a pre-normal load (P_0) is applied to the rail pad, and a uniform contact stiffness (k_c) is modeled at all of its contact nodes. The normal load ($N = P_0 - k_c u_3$) is determined by normal load variation ($F_s = k_c u_3$) and pre-stress ($P = P_0 / A_c$).

The displacement vector ($\mathbf{u}$) and velocity vector ($\mathbf{v}$) of the
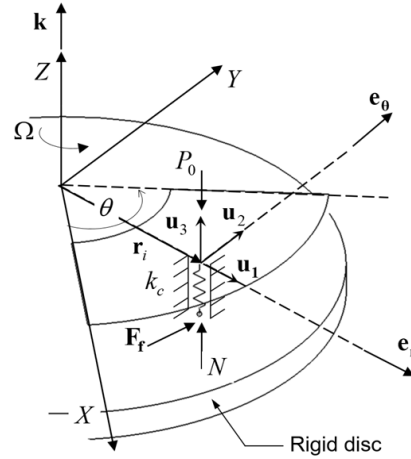

Fig. 4. Contact kinematics of the rail pad.

rail pad can be expressed in global coordinates (X,Y,Z) as:

$$\mathbf{u} = u_1 \mathbf{e_r} + u_2 \mathbf{e_\theta} + u_3 \mathbf{k} \tag{1}$$

$$\mathbf{v} = \dot{u}_1 \mathbf{e_r} + \dot{u}_2 \mathbf{e_\theta} + \dot{u}_3 \mathbf{k}. \tag{2}$$

The relative velocity vector at a contact node is:

$$\mathbf{v_{rel}} = \mathbf{v} - \mathbf{v_d}. \tag{3}$$

Here, $\mathbf{v_d}$ denote sliding velocity of disc at contact point.

From Coulomb's law of friction, the contact friction force vector is expressed as:

$$\mathbf{F_f} = -\frac{\mathbf{v_{rel}}}{|\mathbf{v_{rel}}|} \cdot \mu \cdot N. \tag{4}$$

To capture the negative slope effect, the friction curve is expressed as:

$$\mu(\mathbf{v_{rel}}) = \mu_k + (\mu_s - \mu_k)e^{-h|\mathbf{v_{rel}}|} \tag{5}$$

where μ_k and μ_s are the dynamic friction coefficient and static friction coefficient, respectively, and h is the decay coefficient. These control parameters determine the negative slope of the friction-velocity curve at the rail pad.

All vibration modes of the rail pad are expressed with modal expansion, which is extracted by n-number of nodes and N-number of modes using the assumed mode method ((n = 4588), (N = 55)).

$$\mathbf{u_1} \cong \left[\phi_{ij}^r \right]\{q_j\} = \sum_{i=1}^{n}\sum_{j=1}^{N} \phi_{ij}^r \mathbf{q}_j,$$

$$(i = 1, 2, \cdots, n), (j = 1, 2, \cdots, N) \tag{6}$$

$$\mathbf{u_2} \cong \left[\phi_{ij}^\theta \right]\{q_j\} = \sum_{i=1}^{n}\sum_{j=1}^{N} \phi_{ij}^\theta \mathbf{q}_j \tag{7}$$

$$\mathbf{u}_3 \cong \left[\phi_{ij}^z\right]\{q_j\} = \sum_{i=1}^{n}\sum_{j=1}^{N}\phi_{ij}^z \mathbf{q}_j \qquad (8)$$

where the superscripts r, θ and z represent the directions of the normal, tangential and transverse direction respectively, and the subscripts i and j denote the i th node and j th mode, respectively. Here, ϕ_{ij}^r, ϕ_{ij}^θ and ϕ_{ij}^z are matrices of the eigenfunctions extracted from each direction. The coordinate $\mathbf{q}_j$ is the modal coordinate of the j th mode, and modal coordinates $\mathbf{q} = \{q_1, q_2, q_3, \cdots, q_j, \cdots q_N\}^T$ are rearranged in a vector form for the following discretization.

From the discretization of the Lagrange equation by modal coordinates, the friction-coupled equations of motion are:

$$\frac{d}{dt}\left[\frac{\partial T}{\partial \dot{q}_j}\right] - \left[\frac{\partial T}{\partial q_j}\right] + \left[\frac{\partial U}{\partial q_j}\right] = \sum_{g=1}^{N}Q_{jg}, \qquad (9)$$
$$(j = 1,2,3,\cdots,N),(g = 1,2,3,\cdots,N)$$

$$\delta W \equiv \sum_{j=1}^{N}\sum_{g=1}^{N}Q_{jg}\delta q_j \qquad (10)$$

where U and T are the total strain energy and the total kinetic energy of the uncoupled rail pad, respectively, which are obtained from FEA. Furthermore, Q and δW denote the generalized force term and total virtual work ($\delta W = \delta W_s + \delta W_f$), respectively.

The virtual work of the rail pads can be expressed as follows using the conservative virtual work (δW_s) by the contact stiffness and the non-conservative virtual work (δW_f) by the friction force.

$$\delta W_s = -\int_A (k_c \mathbf{u}_3) \cdot \delta \mathbf{u}_3 \, dA \qquad (11)$$

$$\delta W_f = \int_A \mathbf{F_f} \cdot (\delta \mathbf{u}_1 + \delta \mathbf{u}_2) \, dA \qquad (12)$$

The contact friction force vector expressed by Eq. (4) is linearized by Taylor expansion at steady sliding equilibrium such that:

$$\mathbf{F_f} = -\frac{1}{\Omega r}\mu_0 N \dot{u}_1 \mathbf{e_r} + (\mu_0 N + \alpha N \dot{u}_2)\mathbf{e_\theta} + h.o.t \qquad (13)$$

where r is the radius of disc, μ_0 is friction coefficient at steady sliding equilibrium, α is value of linearized negative slope, and $h.o.t$ denotes higher order terms. From the mass-normalization and the linearization at the steady sliding equilibrium of Eq. (9), the homogeneous part of the linearized equations of motion takes a matrix form ($N \times N$) such that:

$$[I]\{\ddot{q}\} + ([N_d] + [F_d] + [M_d])\{\dot{q}\}$$
$$+ ([\omega^2] + [k_c] + [A])\{q\} = \{0\}. \qquad (14)$$

The physical meaning of each system matrix of Eq. (14) is provided in the following. The matrix $[\omega^2]$ is the diagonal matrix ($[\omega^2] = [\omega^2]^T$) of the natural frequency, the matrix $[k_c]$ is the stiffness-coupled matrix ($[k_c] = [k_c]^T$), and the matrix $[A]$ is the friction-coupled matrix ($[A] \neq [A]^T$). The matrix $[N_d]$ is a negative damping matrix from the negative slope effect ($[N_d] = [N_d]^T$), the matrix $[F_d]$ is a friction damping matrix form the radial dissipative effect ($[F_d] = [F_d]^T$), and the matrix $[M_d]$ is a modal damping matrix from structure damping ($[M_d] = [M_d]^T$). The components of the matrices of Eq. (14) are:

$$[\omega^2] = diag[\omega^2_i] \qquad (15)$$

$$[M_d] = diag[2\xi_i \omega_i] \qquad (16)$$

$$[k_c] = \int_A k_c \sum_i^n \sum_j^N \phi_{ij}^z \cdot \sum_p^n \sum_g^N \phi_{pg}^z \, dA \qquad (17)$$

$$[A] = \int_A \mu_0 k_c \sum_i^n \sum_j^N \phi_{ij}^z \cdot \sum_p^n \sum_g^N \phi_{pg}^\theta \, dA \qquad (18)$$

$$[N_d] = \int_A -\alpha P \sum_i^n \sum_j^N \phi_{ij}^\theta \cdot \sum_p^n \sum_g^N \phi_{pg}^\theta \, dA \qquad (19)$$

$$[F_d] = \int_A \frac{1}{r_i \Omega}\mu_0 P \sum_i^n \sum_j^N \phi_{ij}^r \cdot \sum_p^n \sum_g^N \phi_{pg}^r \, dA. \qquad (20)$$

The numerical integrations of the contact area [17] are available in such a way that:

$$\int_A (\bullet)dA = \int_\theta \int_r (\bullet) \cdot r \cdot dr \cdot d\theta = \sum_{a=1}^{N_r}\sum_{b=1}^{N_\theta}(\bullet) \cdot r_a \cdot \Delta r_a \cdot \Delta \theta_b \qquad (21)$$

where N_r and N_θ are the number of nodes in the radial direction and theta direction in the contact area, respectively.

The component eigenvectors and eigenvectors of the coupled systems are:

$$\mathbf{w}^0 = \left\{\mathbf{w}_1^0, \mathbf{w}_2^0, \cdots, \mathbf{w}_j^0, \cdots, \mathbf{w}_N^0\right\} \qquad (22)$$

$$\mathbf{w} = \left\{\mathbf{w}_1, \mathbf{w}_2, \cdots, \mathbf{w}_j, \cdots, \mathbf{w}_N\right\} \qquad (23)$$

where $\mathbf{w}^0$ is the orthonormal unit vector of the uncoupled system ($k_c = 0$), and $\mathbf{w}$ is the normalized orthonormal eigenvector of the coupled system ($k_c \neq 0$). By modal expansion, the j th normalized orthonormal eigenvector of the coupled system can be expressed as follows.

$$\mathbf{w}_j = C_{j1}\mathbf{w}_1^0 + C_{j2}\mathbf{w}_2^0 + \cdots + C_{ji}\mathbf{w}_j^0 + \cdots + C_{jn}\mathbf{w}_N^0 \qquad (24)$$

In the matrix form constructing modal matrix,

$$\begin{bmatrix}\mathbf{w}_1 & \cdots & \mathbf{w}_n\end{bmatrix} = \begin{bmatrix}\mathbf{w}_1^0 & \cdots & \mathbf{w}_n^0\end{bmatrix}\begin{bmatrix} C_{11} & \cdots & C_{1n} \\ \vdots & \ddots & \vdots \\ C_{N1} & \cdots & C_{Nn}\end{bmatrix} \qquad (25)$$

$$[\Phi] = [\Phi^0][C] \qquad (26)$$

or equivalently,

$$[C] = \left[\Phi^0\right]^{-1}[\Phi] \tag{27}$$

where

$$\left[\Phi\right] = \left[\mathbf{w}_1 \quad \cdots \quad \mathbf{w}_N\right] \tag{28}$$

$$\left[\Phi^0\right] = \left[\mathbf{w}_1^0 \quad \cdots \quad \mathbf{w}_N^0\right] \tag{29}$$

$$[C] = \left[C_{ji}\right] \tag{30}$$

where the modal matrices for $\mathbf{w}^0$ and $\mathbf{w}$ are defined as $\left[\Phi^0\right]$ and $\left[\Phi\right]$, respectively. The modal contribution matrix for C is defined as $[C]$. The subscript j denote the j th mode, and C_{ji} is a component of the orthogonal unit vector corresponding to $\mathbf{w}_{j(i)}^0$. Since the eigenvectors of the uncoupled system ($\mathbf{w}^0$) form a standard basis, the eigenvectors of the coupled system ($\mathbf{w}$) can be expressed in a linear combination, and corresponding scalar (C_{ji}) exists. In other word, the eigenvector is linearly independent. Therefore, the scalar C_{ji} is component of standard basis and indicates how much $\mathbf{w}^0$ contributes to $\mathbf{w}$.

The modal contribution factor (MCF) is useful to predict mode shape of coupled system. The MCF was calculated for mode-tracking of the increase of contact stiffness in rigid mode. The j th column of $[C]$ is the MCF to the j th mode of coupled system. Eq. (27) is solved for increases in contact stiffness, for which we can express the MCF of each mode.

3. Results

To find the dominant mode that produces the squeal propensity in the rail pad, we analyzed the contact stiffness variation of 10 modes. The range of contact stiffness is 0 to 100 %, and the frequency change of the rigid mode reaches 5000 Hz. The stiffness-coupled system equation with $\mu = 0$ to track the mode shape changes for contact stiffness increases is:

$$[I]\{\ddot{q}\} + \left([\omega^2] + [k_c] + [A]\right)\{q\} = \{0\} . \tag{31}$$

As shown in Fig. 5(a), we focused on the mode locus of the z-translation mode (A_1).

Fig. 5(c) shows the mode shape when the contact stiffness for mode A_1, A_2, B_1, C_1, and D_1 is zero. These represent the z-translation mode A_1 (0 Hz), 1st flexible mode A_2 (986 Hz), 4th flexible mode B_1 (2114 Hz), 9th flexible mode C_1 (3349 Hz), and 10th flexible mode D_1 (3588 Hz), respectively. Fig. 5(b) shows the region with Re > 0, and the value of the boundary is called the critical friction coefficient. The z-translation mode is greatly increased in frequency along the mode locus when the contact stiffness is increased. Particularly, the critical friction coefficient at I, II, and III sharply decreases. Thus, mode-veering and mode-exchanging are shown in Figs. 6-8 using frequency variation and MCF at positions I, II, and III with high squeal propensity.

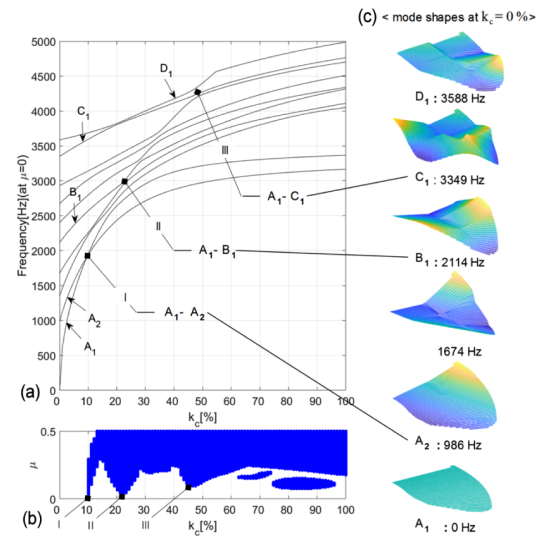Figs. 6-8(a) show the frequency variation generating the

Fig. 5. Eigenvalue sensitivity analysis: (a) frequency loci with respect to contact stiffness; (b) squeal propensity; (c) mode shape.
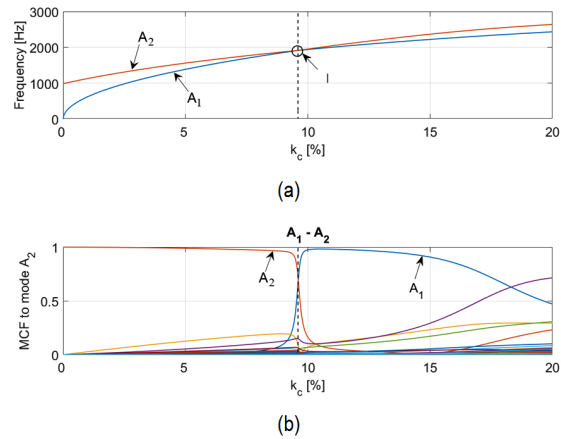

Fig. 6. Mode veering and mode exchanging at I: (a) frequency loci of two mode; (b) MCF.

mode-veering mode at points I, II, and III. Figs. 6-8(b) show the MCF corresponding to the frequency variation. At each point of I, II, and III, the frequencies of z-translation mode and flexible mode are very close and the MCF crosses. In other words, mode-veering and mode-exchanging occur at these points. Mode-exchanging contributes significantly to the z-translation mode, as seen at each point.

Continuous changes of the z-translation mode are shown in Fig. 8(b). The mode-veering phenomenon is complicated at III. Mode-exchanging of mode C_1 and mode D_1 occurs near the initial contact stiffness of 23 %, and the contribution to mode C_1 is increased. However, as contact stiffness increases, the contribution to mode C_1 gradually decreases. In addition, as the contact stiffness increases, the z-translation mode increases continuously in frequency and produces new mode-exchanging and mode-veering with mode C_1 at around 45 % of contact stiffness.
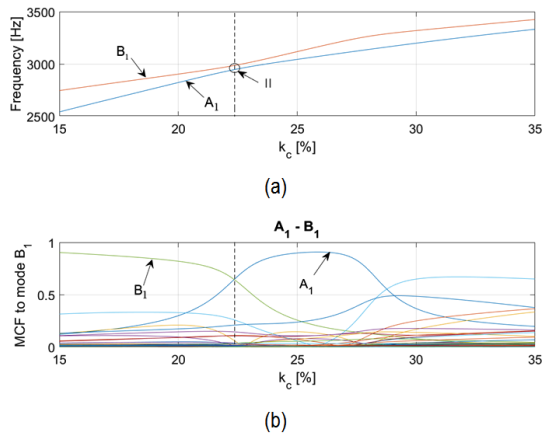
The results from the MCF of z-translation mode are pre-

(a)

(b)

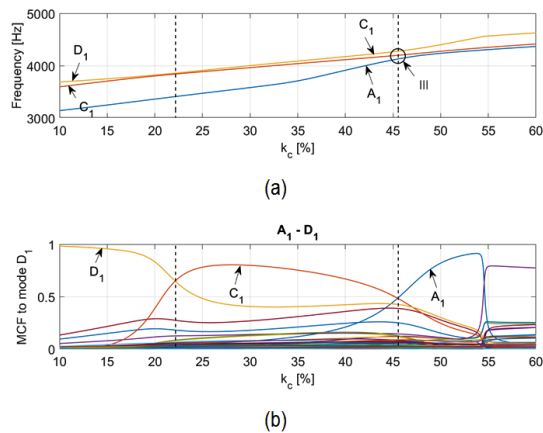Fig. 7. Mode veering and mode exchanging at II: (a) frequency loci of two mode; (b) MCF.

(a)

(b)

Fig. 8. Mode veering and mode exchanging at III: (a) frequency loci of two mode; (b) MCF.

Fig. 9. Stability map for the friction coefficient, where "blue thick curve" indicates positive real part: (a) frequency loci at I (k_c = 9.5 %); (b) real part at I (k_c = 9.5 %); (c) frequency loci at II (k_c = 22.5 %); (d) real part at II (k_c = 22.5 %); (e) frequency loci at III (k_c = 45.5 %); (f) real part at III (k_c = 45.5 %).

dominantly indicated. The z-translation mode has a frequency of 0 Hz when the initial contact stiffness is zero. However, as the contact stiffness increases, the frequency of the z-translation mode increases, which implies that the mode is constantly changing. In other words, this z-translation mode changes mode along a specific mode locus and as the frequency increases. The sensitivity to dynamic instability is maximized at the point of mode-veering and mode-exchanging. This suggests that the squeal propensity for the rail pad changes with the locus of the z-translation mode, as shown in Fig. 5.

The analysis of mode-coupling instability for the z-translation was performed by selecting the friction coefficient as a parameter at positions I, II, and III (mode-veering). The results are shown in Fig. 9. Figs. 9(a), (c) and (e) show the frequency loci for the friction coefficients of the major modes (A_1, A_2, B_1, C_1) at points I, II, and III. Figs. 9(b), (d) and (f) show the corresponding real parts of the loci. Mode-veering was created by the mode-merging of the changed z-translation mode and flexible mode at very low critical friction coefficients. In conclusion, the mode-coupling instability of the rail pad is produced
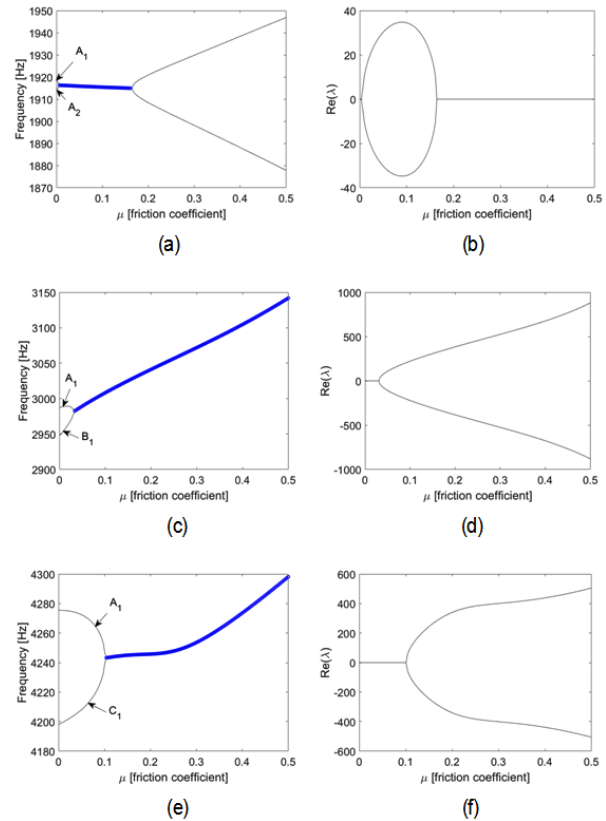
by the mode-veering at a very low critical friction coefficient. This implies that the major mode for generating the dynamic instability is the z-translation mode with the increase in the contact stiffness.

4. Discussion and conclusions

In this study, the dynamic instability of a rail pad was predicted using a semi-analytical model. The mechanism of dynamic instability was described with a focus on the mode-coupling mechanism of the z-translation mode and flexible mode. This was achieved by conducting an eigenvalue sensitivity analysis and modal contribution analysis. The z-translation mode is the main mode of generating mode-coupling instability in the rail pad. The z-translation mode greatly increases in frequency with increasing contact stiffness, resulting in mode-coupling instability with many flexible modes. Therefore, we predict that the z-translation mode in the rail pad is the main mode for generating squeal propensity.

References

[1] G. X. Chen, Z. R. Zhou, P. Kapsa and L. Vincent, Experimental

investigation into squeal under reciprocating sliding, *Tribology International*, 36 (12) (2003) 961-971.

[2] N. Fan and G. X. Chen, Numerical study of squeaking suppresses for ceramic-on-ceramic hip endoprosthesis, *Tribology International,* 48 (2012) 172-181.

[3] B. C. Goo and J. C. Kim, Complex eigenvalue analysis of railway wheel/rail squeal, *International Journal of Engineering Science and Technology*, 8 (1) (2016) 1-12.

[4] H. Ouyang, W. Nack, Y. Yuan and F. Chen, Numerical analysis of automotive disc brake squeal: A review, *International Journal of Vehicle Noise and Vibration*, 1 (3-4) (2005) 207-231.

[5] F. Massi, G. Oliviero and L. Baillet, Brake squeal as dynamic instability: An experimental investigation, *The Journal of the Acoustical Society of America*, 120 (3) (2006) 1388-1398.

[6] J. Nam and J. Kang, Brake squeal analysis with respect to caliper contact stiffness, *Transactions of the Korean Society for Noise and Vibration Engineering*, 23 (8) (2013) 717-724.

[7] E. Denimal, S. Nacivet, L. Nechak and J. J. Sinou, On the influence of multiple contact conditions on brake squeal, *Procedia Engineering*, 199 (2017) 3260-3265.

[8] C. Kim, Y. Kwon and D. Kim, Analysis of low-frequency squeal in automotive disc brake by optimizing groove and caliper shapes, *International Journal of Precision Engineering and Manufacturing*, 19 (4) (2018) 505-512.

[9] F. Cascetta, F. Caputo and A. D. Luca, Squeal frequency of a railway disc brake evaluation by FE analyses, *Advances in Acoustics and Vibration* (2018).

[10] A. Belhocine and N. M. Ghazaly, Effects of Young's modulus on disc brake squeal using finite element analysis, *International Journal of Acoustics and Vibration*, 21 (3) (2016) 292-300.

[11] Y. Du and Y. Wang, Squeal analysis of a modal-parameter-based rotating disc brake model, *International Journal of Mechanical Sciences*, 131 (2017) 1049-1060.

[12] S. Nacivet and J. J. Sinou, Modal amplitude stability analysis and its application to brake squeal, *Applied Acoustics*, 116 (2017) 127-138.

[13] J. Nam, H. Do and J. Kang, Investigation of friction induced vibration in lead screw system using FE model and its experimental validation, *Applied Acoustics*, 122 (2017) 98-106.

[14] J. Nam, H. Choi and J. Kang, Finite element analysis for friction noise of simplified hip joint and its experimental validation, *Journal of Mechanical Science and Technology*, 30 (8) (2016) 3453-3460.

[15] J. Kang, Squeal analysis of gyroscopic disc brake system based on finite element method, *International Journal of Mechanical Sciences*, 51 (4) (2009) 284-294.

[16] J. Kang, Finite element algorithm reproducing hip squeak measured in experiment, *Journal of Sound and Vibration*, 393 (2017) 374-387.

[17] J. Kang, Automotive brake squeal analysis with rotating finite elements of asymmetric disc in time, *Journal of Sound and Vibration*, 393 (2017) 388-400.

[18] J. J. Sinou, A. Loyer, O. Chiello, G. Mogenier, X. Lorang, F. Cocheteux and S. Bellaj, A global strategy based on experiments and simulations for squeal prediction on industrial railway brakes, *Journal of Sound and Vibration*, 332 (20) (2013) 5068-5085.

[19] S. Hsu, Z. Huang, S. Iwnicki, D. Thompson, C. Jones, G. Xie and P. Allen, Experimental and theoretical investigation of railway wheel squeal, *Proceedings of the Institution of Mechanical Engineers, Part F: Journal of Rail and Rapid Transit*, 221 (1) (2007) 59-73.

[20] X. Liu and P. Meehan, Wheel squeal noise: A simplified model to simulate the effect of rolling speed and angle of attack, *Journal of Sound and Vibration*, 338 (2015) 184-198.

[21] J. F. Brunel, P. Dufrénoy and F. Demilly, Modelling of squeal noise attenuation of ring damped wheels, *Applied Acoustics*, 65 (5) (2004) 457-471.

[22] S. De, Z. Rivera and D. Guida, Finite element analysis on squeal-noise in railway applications, *FME Transactions*, 46 (1) (2018) 93-100.

[23] J. Kang, C. M. Krousgrill and F. Sadeghi, Analytical formulation of mode-coupling instability in disc–pad coupled system, *International Journal of Mechanical Sciences*, 51 (1) (2009) 52-63.

[24] J. Kang, Squeal propensity due to rigid modes of brake pad, *Proceedings of the Institution of Mechanical Engineers, Part C: Journal of Mechanical Engineering Science*, 228 (12) (2014) 2100-2109.

[25] B. Goo, Analysis of unstable vibration modes due to KTX brake disc/pad interaction, *Journal of the Korean Society for Railway*, 16 (4) (2013) 253-261.

[26] J. Kang, Analytical approach for modal instability of a rigid brake pad, *Proceedings of the Institution of Mechanical Engineers, Part D: Journal of Automobile Engineering*, 229 (6) (2015) 719-727.

[27] J. Huang, C. M. Krousgrill and A. K. Bajaj, Modeling of automotive drum brakes for squeal and parameter sensitivity analysis, *Journal of Sound and Vibration*, 289 (1-2) (2006) 245-263.

Jaeyoung Kang is a Professor in the Department of Mechanical Engineering, Inha University. He received his Ph.D. degree in Mechanical Engineering from Purdue University in 2008. His research interests include friction noise, structural vibration and nonlinear dynamics.